

## Nanoplasmonic Photoelectron Rescattering in the Multiphoton-Induced Emission Regime

Balázs Bánhegyi,<sup>1,2</sup> Gellért Zsolt Kiss,<sup>1</sup> Zsuzsanna Pápa<sup>1,3</sup>, Péter Sándor<sup>1</sup>, Lázár Tóth,<sup>3</sup>

László Péter<sup>1</sup>, Péter Rácz,<sup>1,\*</sup> and Péter Dombi<sup>1,3,†</sup>

<sup>1</sup>*HUN-REN Wigner Research Centre for Physics, 1121 Budapest, Hungary*

<sup>2</sup>*Budapest University of Technology and Economics, 1111 Budapest, Hungary*

<sup>3</sup>*ELI-ALPS Research Institute, 6728 Szeged, Hungary*



(Received 16 July 2023; accepted 4 June 2024; published 15 July 2024)

In strong-field laser-matter interactions, energetic electrons can be created by photoemission and a subsequent rescattering and can attain energy as much as 10 times the ponderomotive potential ( $U_p$ ) of the laser field. Here, we show that with the unique combination of infrared laser sources (exploiting the quadratic scaling of  $U_p$ ) and plasmonic nanoemitters (which enhance rescattering probability by orders of magnitude)  $\sim 10U_p$  rescattered electrons can be observed in the multiphoton-induced regime. Our experiments correspond well to a model based on the time dependent Schrödinger equation and allowed us to reveal an unexpected aspect of ultrafast electron dynamics in the multiphoton emission regime.

DOI: [10.1103/PhysRevLett.133.033801](https://doi.org/10.1103/PhysRevLett.133.033801)

*Introduction.*—The photoionization of atoms and molecules under intense laser irradiation unraveled many intriguing phenomena, both at the low-intensity and high-intensity extremes, laying the foundations for important research fields such as attosecond science [1]. Investigations at lower field strengths led to the observation of the above-threshold ionization [2] and paved the way to its full quantum mechanical explanation by multiphoton absorption [3–5]. Strong-field interactions at higher intensity laser fields were discussed using the semiclassical simple man’s theory [6–8] combined with a quantum-mechanical approach by Keldysh, Faisal, and Reiss [9–11].

Over the past years, interest in strong-field interactions has spread out into the realm of metallic nanotips, surfaces, and plasmonic nanostructures resulting in the emergence of strong-field nano-optics [8,12]. Experiments involved ponderomotive and subcycle electron acceleration [13–15], photoassisted tunneling [16], carrier-envelope effects [17,18], ultrasensitive probing of hot electron occupancies [19], and electron emission from nanotips for ultrafast electron microscopy–diffraction applications [20–22]. The unique optical properties of plasmonic nanostructures, such as their ability to concentrate light into subwavelength domains, and the substantial enhancement of local fields at their surface make them ideal platforms for probing nonlinear optical processes at the nanoscale, such as observing strong-field photoemission [23], measuring plasmonic field enhancement [24–26], and resolving the transition between the previously mentioned photoemission regimes [27]. All these fundamental observations contributed to a deeper understanding of plasmonic light-matter interactions [28–30].

Photoionization and photoemission electron spectra have fundamental features in common. If the laser field perturbs

atomic or surface potentials only slightly, triangle-shaped electron spectra can be observed on a semilogarithmic plot, owing to the exponentially decaying part which has a well-defined  $2U_p$  cutoff energy [31,32]. In the strong-field regime the higher intensity laser field distorts the local atomic-surface potential to such an extent that tunneling of the electrons becomes possible. The resulting photoelectron spectra have a plateau, with an unmistakable roll-off part starting at  $10U_p$  cutoff energy [33]. In the spectra, the plateau can be attributed to the phenomenon where photoemitted electrons are driven back in the near field to the emission surface from which they rescatter, thereby gaining high energy [33,34].

In atomic and molecular physics, the transition is intuitively expected at values of the order of  $\gamma \approx 1$  of the Keldysh parameter [35,36] with  $\gamma = \sqrt{W/2U_p}$ , where  $W$  is the ionization potential of the atom (or, for solids, the work function of the metal), and  $U_p$  is the cycle-averaged kinetic energy—or ponderomotive energy—of a free electron in the field of an electromagnetic wave. For solid photoemission targets, such as metallic surfaces, the transition region between the multiphoton-induced and strong-field emission regime was reported to be at  $\gamma \approx 1$ –2.3 [37,38]. In the case of sharp metallic tips, the transition region was identified at  $\gamma \approx 2$  [22]. For lower Keldysh- $\gamma$  values, the proportion of the electrons experiencing recollision events with the nanostructure surface with respect to the electrons directly leaving the near field will increase, resulting in well-defined plateaus in the photoelectron spectra with a high-energy cutoff, that follows the  $10U_p$  scaling law [27]. This clear separation of the lower energy  $2U_p$  and high energy  $10U_p$  electrons based on the photoelectron spectra was

widely accepted and has been used previously in several studies [13,17,38–42].

Contrary to previous expectations, here we report on observations that  $10U_p$  rescattering effects are also present deep in the multiphoton-induced photoemission regime, up to Keldysh- $\gamma$  values of 5, extending our understanding of strong-field and quasi-strong-field interactions. The observation of the rescattering process in the multiphoton regime is enabled by the unique combination of two concepts which renders the measurement of  $10U_p$  electrons easy for lower intensities. (i) We employed midinfrared laser pulses exploiting the quadratic scaling of  $U_p$  with wavelength so that cutoffs are shifted to the 3–15 eV range even at low intensities, rendering measurements with a suitable time-of-flight spectrometer feasible. (ii) Instead of atoms, we used plasmonic nanoparticles as rescattering targets. This is absolutely essential since midinfrared excitation drastically reduces the probability of rescattering for atoms [43]. That is the reason why this effect was not observed previously in atomic physics experiments. However, by employing plasmonic nanoparticles as photoemission sources the returning wave packet can efficiently rescatter at the extended surface of the nanoparticle rendering the rescattered electrons measurable above the noise floor.

Our observations are well supported by theory based on the time dependent Schrödinger equation modeling of photoelectron spectra.

*Theoretical background of electron rescattering and results.*—For the understanding of theoretical and experimental results, we used the following formula for the Keldysh parameter derived from the definition of the ponderomotive energy ( $U_p = e^2 I / 2c\epsilon_0 m_e \omega_0^2$ , where  $e$  and  $m_e$  are the charge and mass of an electron,  $c$  is the speed of light,  $\epsilon_0$  is the vacuum permittivity,  $\omega_0$  is the frequency,  $I$  is the intensity of the local electromagnetic field, and  $E$  is the corresponding local electric field strength):  $\gamma = \omega_0 \sqrt{2W} / E = \eta / (\lambda \sqrt{I})$ , where  $\eta = 2\pi \sqrt{W c^3 \epsilon_0 m_e} / e \approx 537.4$  [ $\text{m} \sqrt{\text{kg}/\text{s}^3}$ ] is a constant comprised of only natural constants and the ionization potential of an atomic electron or the work function of the metal ( $W$ ). From this point on, we will use the notation  $\gamma_{\text{loc}}$  for Keldysh- $\gamma$  to indicate that we take local, plasmonically enhanced electric field values in the closest, nanoscale vicinity of the nanoparticles where rescattered electrons are accelerated to their final energies.

In order to investigate the presence of rescattered electrons and to quantify their contribution in the photoelectron spectra obtained for the considered local field regimes we employed the already well-documented split-operator Crank-Nicolson approach [37,44], and solved the time-dependent 1D-Schrödinger equation [ $i\hbar \partial \Psi(z; t) / \partial t = H(t) \Psi(z; t)$ ] within the single active electron approximation (SAE). The full detailed description of the method, the considered potentials, and the splitting of the wave function (so that rescattered electrons can be made visible) can be

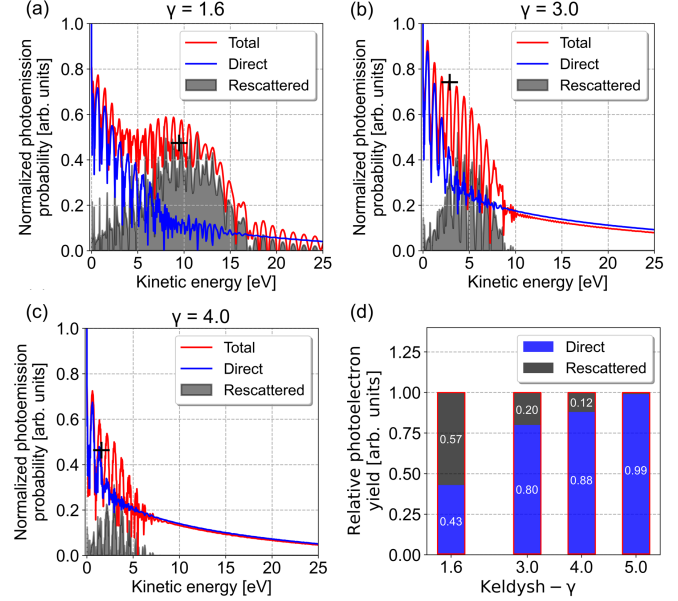


FIG. 1. (a)–(c) Calculated photoemission spectra based on the time-dependent Schrödinger equation for multi-cycle 27-fs, 1600-nm driver pulses composed of 5 optical cycles (intensity full width at half maximum). Keldysh- $\gamma$  values are calculated for plasmonenhanced local fields since electron quiver amplitudes are on the order of few nanometers. The continuous red lines indicate results from the full wavefunction containing both direct and rescattered electrons. The blue lines show spectra of direct electrons, and the black lines show spectra of rescattered electrons. The black cross shows the position of the  $10U_p$  energy calculated using the local field properties and natural parameters. (d) Calculated relative photoelectron yields showing the amount of direct and rescattered electrons for increasing Keldysh- $\gamma$  values.

found in Supplemental Material [45]. The laser fields were 5-cycle pulses at 1600 nm central wavelength, and their field strengths were chosen in such a way that first, we started from a quasi-strong-field case [Fig. 1(a)], where a well-distinguishable plateau region can be identified in the final spectra (i.e.,  $\gamma_{\text{loc}} = 1.6$ ). Then, we gradually decreased the field amplitude with increasing Keldysh- $\gamma$  values up to 5 [Figs. 1(b)–1(d)]. Here—for better visibility—the calculated photoelectron signal was defined by normalizing the logarithm of the photoemission probability densities ( $P_s$ —for further description, see Supplemental Material [45]).

In the total electron signal of the  $\gamma_{\text{loc}} = 1.6$  result in Fig. 1(a), we see a large contribution of the rescattered electrons (black lines) which appears in the total spectra as a well-distinguishable plateau, that expands from  $2U_p$  up to  $10U_p$ , confirming the cutoff law of  $E_{\text{cutoff}} \sim 10U_p$  followed by the well-known roll-off. With the decrease of the field amplitude to  $\gamma_{\text{loc}} = 3$  a small plateau remains still observable. To quantify the contribution of rescattered electrons to the final photoelectron spectra, the ratio of direct and rescattered electrons to the total electron yield was also calculated [Fig. 1(d)]. Toward the two lowest intensities

one can see in Figs. 1(c) and 1(d) that the contribution from the rescattered electrons start to rapidly fade away, but for  $\gamma_{\text{loc}} = 4$  it still has a small impact on the total electron signal. The presence of rescattered electrons vanishes for  $\gamma_{\text{loc}} > 5$ , with the proportion of rescattered electrons being  $\sim 1\%$  for the threshold value of  $\gamma_{\text{loc}} = 5$ . This is exactly what we see in our experiments below, namely the presence of rescattering electrons for focused local intensity values corresponding to  $\gamma_{\text{loc}} \sim 5$ .

Since we used a 1D model, we cannot take into account the geometric effects of the nanoparticle, but in this case, this is not a fundamental factor, because of the quiver amplitude of the electrons during the acceleration process is in the subnanometer range, the backscattering also occurs at this scale. The sizes of the nanoparticles in our experiments are much larger ( $\sim 100$  nm), hence we do not expect that the ratio of rescattered electrons depends significantly on the size and the geometry of the nanoparticles [8]. Geometrical effects have influence on the value of the maximum field enhancement, which was considered in our FDTD calculations aimed at resolving the local field distribution at the emission sites.

*Experimental probing of rescattering in the multiphoton regime.*—After the theoretical foundations, we can approach the details of our experimental setup used to investigate the aforementioned rescattering in the multiphoton regime from plasmonic nanostructures. Using longer wavelength pulses from a femtosecond optical parametric amplifier between  $1.6 \mu\text{m}$  and  $2.4 \mu\text{m}$ —combined with the use of plasmonic resonance—we can reach higher local peak intensities and thus, lower Keldysh-parameters at lower incident intensities, thereby avoiding extensive material damage. In order to overcome the issue of exceptionally low rescattering probability—which is specific to atomic targets—we employ plasmonic nanostructures as photoemission targets as discussed above. The laser system is based on a regenerative amplifier system that provides 40-fs pulses at a 10-kHz repetition rate with pulse energies of  $> 300 \mu\text{J}$ . The pulses are directed into an optical parametric amplifier system, generating 70-fs pulses with central wavelengths between  $1.6 \mu\text{m}$  and  $2.4 \mu\text{m}$ , in our case.

These infrared pulses were focused into the vacuum chamber (pumped by turbomolecular pumps to a base pressure of around  $10^{-7}$  mbar) housing the photoemission targets on a three-dimensional, closed-loop piezoelectric nanopositioner. The emitted electrons were detected using a time-of-flight spectrometer (Kaesdorf ETF10) with drift-tube voltage set to 20 V, equipped with a microchannel plate (MCP) detector. The electron signal of the MCP was registered using a high-speed measurement card (FASTComTec MCS6A). The resulting TOF spectra were transformed into photoelectron kinetic energy spectra using the measured calibration curve of the spectrometer.

The photoemission targets were gold nanorods with sizes of  $570 \times 115$  nm in a two-dimensional array layout with

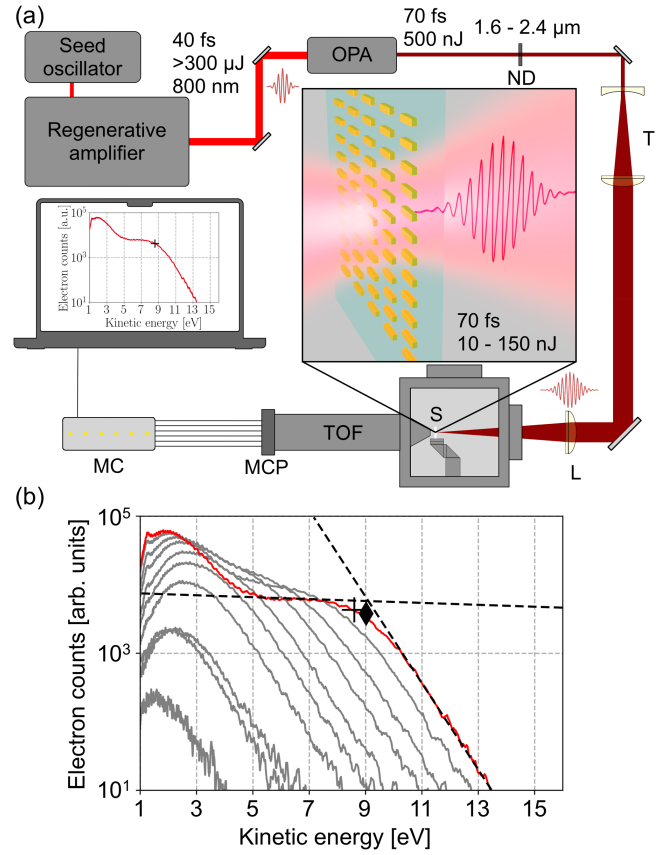


FIG. 2. (a) Experimental setup, containing the femtosecond light source, the time-of-flight spectrometer (TOF), and the high-speed measurement card (MC). Further components: neutral density filters (ND), Galilean telescope (T), focusing  $\text{CaF}_2$  lens (L), nanostructured array sample (S), microchannel plate detector (MCP). (b) Cutoff definition based on the 99.5% of total electron population (black cross) compared to the conventional method based on the intersection of linear fits (black diamond) in case of a typical electron spectrum series for  $1.6 \mu\text{m}$  incident pulses. inset: nanorod array sample with focusing geometry.

$1 \times 2 \mu\text{m}$  grating constant, manufactured via electron-beam lithography on a fused silica substrate with indium-tin-oxide (ITO) conducting layer [Fig. 2(a) inset]. In order to obtain the plasmonic properties of the nanorods, we performed FDTD simulations (Lumerical FDTD Solutions) for all three wavelengths (for further information, see Supplemental Material [45]). The maximal field enhancement values obtained from these simulations are 15.9, 19.1, and 11.7 for 1600 nm, 2000 nm, and 2400 nm wavelengths, respectively. These results are used for the evaluation of the measured photoelectron spectra.

The obtained spectra for increasing incident intensities with the corresponding local peak intensities (considering the field enhancement) and local Keldysh parameters are shown in Fig. 3(a) for all three applied wavelengths. Looking at the photoelectron data, the characteristic change in the shape of the emission spectra with increasing local intensities is clearly visible. In the case of lower local

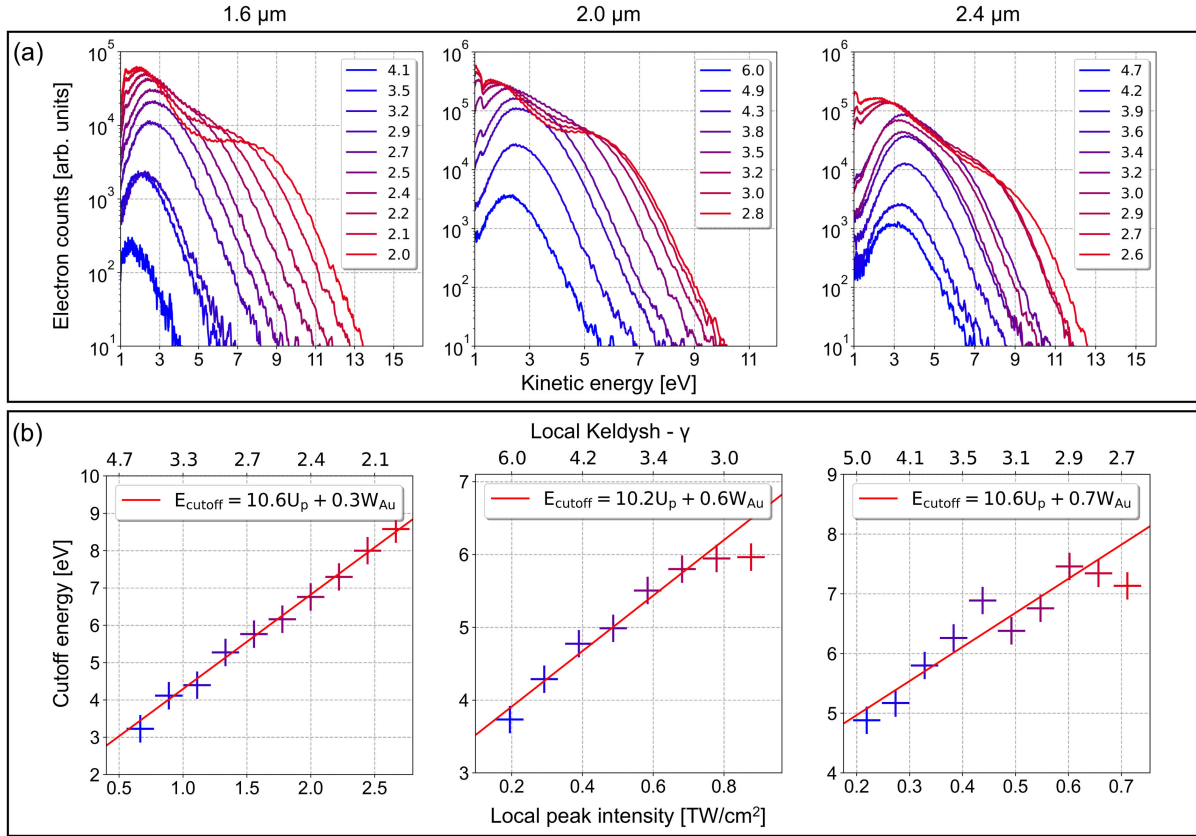


FIG. 3. (a) Photoelectron spectra obtained at increasing local intensities (considering the field enhancement) using 1.6, 2.0, and 2.4  $\mu\text{m}$  pulses. Local Keldysh parameters are indicated in the figure legends. The appearance of the plateau is clearly visible in all cases indicating the transition from multiphoton to strong-field photoemission regime. (b) Cutoff energies plotted against the local peak intensities with the corresponding  $U_p$  scaling acquired from the linear fit. Note that the  $10U_p$  scaling law holds up even at lower intensities in the multiphoton-induced emission regime in case of all three wavelengths.

intensities with larger local Keldysh parameters, triangular shaped spectra were observed for all three wavelengths, which is typical for multiphoton-induced photoemission processes. These spectra are mostly composed of direct electrons with a lower cutoff energy. Increasing the local peak intensity, the appearance of plateaus is clearly visible, which is a telltale sign of the transition to the strong-field regime. Here, the rescattering of the electrons starts to take over, resulting in more energetic electrons with kinetic energies between 8 and 14 eV for the different wavelengths. Figure 3(b) suggests a linear increase of final electron energies for higher local peak intensities, which is a clear sign of the evolution of the electron acceleration in the near field.

To verify the above-mentioned transition process, we extracted the cutoff electron energies for each spectrum group and plotted them against the local peak intensity calculated from the incident intensities and the calculated local field enhancement values. As cutoff energy definition, a traditionally used method is based on linear fitting to the plateau region and the higher-energy roll-off region of the spectra [Fig. 2(b)]. The intersection of these linear regressions gives the cutoff position at the certain local intensity.

This method is effective in the case of plateau-shaped spectra, but less useful in the case of the previously mentioned triangular-shaped spectra, where no plateau is visible. Because of this restriction, we chose to use the 99.5% of the total electron population as a cutoff definition, based on another established method used for photoemission experiments [13]. This method allows us to define cutoff energies for triangular spectra associated with the multiphoton regime, as well. Comparing the cutoff position given by this approach and the previously mentioned one for spectra with distinct plateaus, we can conclude that our method gives cutoff values sufficiently close to the traditionally defined ones as seen in Fig. 2(b).

A further justification of our cutoff definition is that plotting the cutoff values against the local peak intensities, their trend results in a  $10U_p$  scaling for the whole range of the investigated  $\gamma_{\text{loc}} = 2.5\text{--}6$  regime (with the range slightly depending on the wavelength). This can be seen in Fig. 3(b) at the high intensity cutoffs measured in the strong-field regime colored with red. This trend is an absolute sign of the presence of the electron rescattering events, which we observed in the multiphoton-induced

emission regime in a previously unprecedented way. Looking at Fig. 3(b) at 2.0 and 2.4  $\mu\text{m}$ , there are only two outlier measurement points for the highest intensities probably due to saturation effects in the TOF spectrometer for higher electron yields.

The fact that the evaluated cutoff points follow the  $10U_p$  scaling even for the triangular shaped spectra for all three wavelengths confirms the presence of energetic rescattered electrons in the multiphoton-induced emission regime.

*Summary.*—In this Letter we presented experimental results on ultrafast nonlinear photoemission from plasmonic nanoparticles excited by femtosecond laser pulses in the infrared region at three different wavelengths. The choice of the laser wavelength (and the application of plasmonic nanoparticles as rescattering targets) enabled the experimental observation of rescattering electrons in the  $\sim 3$ – $10$  eV range strictly following the  $10U_p$  cutoff scaling law. Since we could confirm that for these measurements local Keldysh- $\gamma$  values were in the range of  $\gamma_{\text{loc}} = 2.5$ – $5$ , the rather counterintuitive presence of rescattered electrons in the multiphoton regime was shown in a conspicuous way. These experiments add significant elements to the understanding of the transition regime between strong-field and perturbative light-matter interaction processes and can help the development of metallic nanoemitters for ultrafast electron diffraction [12,20], ultrafast electron microscopy [12,20,48], and plasmonic photocathodes [49] for cutting-edge applications in ultrafast science and experimental methods.

We acknowledge support from a FET Open Grant of the EU (PetaCOM 829153) and National Research, Development, and Innovation Office of Hungary (Projects No. 137373, No. TKP-2021-NVA-04, and No. 2018-1.2.1-NKP-2018-00012).

\*Contact author: racz.peter@wigner.hun-ren.hu

†Contact author: dombi.peter@wigner.hun-ren.hu

- [1] F. Krausz and M. Ivanov, *Attosecond physics*, *Rev. Mod. Phys.* **81**, 163 (2009).
- [2] P. Agostini, F. Fabre, G. Mainfray, G. Petite, and N. K. Rahman, Free-free transitions following six-photon ionization of xenon atoms, *Phys. Rev. Lett.* **42**, 1127 (1979).
- [3] J. E. Bayfield, Excited atomic and molecular states in strong electromagnetic fields, *Phys. Rep.* **51**, 317 (1979).
- [4] Z. Deng and J. H. Eberly, Multiphoton absorption above ionization threshold by atoms in strong laser fields, *J. Opt. Soc. Am. B* **2**, 486 (1985).
- [5] J. H. Eberly, J. Javanainen, and K. Rzażewski, Above-threshold ionization, *Phys. Rep.* **204**, 331 (1991).
- [6] P. Mulser and D. Bauer, *High Power Laser-Matter Interaction*, Springer Tracts in Modern Physics (Springer, New York, 2010), Vol. 238.
- [7] K. Amini *et al.*, Symphony on strong field approximation, *Rep. Prog. Phys.* **82**, 116001 (2019).
- [8] E. Saydanzad, J. Powell, A. Summers, S. J. Robotjazi, C. Trallero-Herrero, M. F. Kling, A. Rudenko, and U. Thumm, Enhanced cutoff energies for direct and rescattered strong-field photoelectron emission of plasmonic nanoparticles, *Nanophotonics* **12**, 1931 (2023).
- [9] M. V. Fedorov and L. V. Keldysh, Ionization in the field of a strong electromagnetic wave, *Sov. Phys. JETP* **122**, 449 (2016), and references therein.
- [10] F. H. M. Faisal, Multiple absorption of laser photons by atoms, *J. Phys. B* **6**, L89 (1973).
- [11] H. R. Reiss, Effect of an intense electromagnetic field on a weakly bound system, *Phys. Rev. A* **22**, 1786 (1980).
- [12] P. Dombi, Z. Pápa, J. Vogelsang, S. V. Yalunin, M. Sivis, G. Herink, S. Schäfer, P. Groß, C. Ropers, and C. Lienau, Strong-field nano-optics, *Rev. Mod. Phys.* **92**, 025003 (2020).
- [13] G. Herink, D. R. Solli, M. Gulde, and C. Ropers, Field-driven photoemission from nanostructures quenches the quiver motion, *Nature (London)* **483**, 190 (2012).
- [14] K. E. Echterkamp, G. Herink, S. V. Yalunin, K. Rademann, S. Schäfer, and C. Ropers, Strong-field photoemission in nanotip near-fields: From quiver to sub-cycle electron dynamics, *Appl. Phys. B* **122**, 80 (2016).
- [15] J. Schötz, S. Mitra, H. Fuest, M. Neuhaus, W. A. Okell, M. Förster, T. Paschen, M. F. Ciappina, H. Yanagisawa, P. Wnuk, P. Hommelhoff, and M. F. Kling, Nonadiabatic ponderomotive effects in photoemission from nanotips in intense midinfrared laser fields, *Phys. Rev. A* **97**, 013413 (2018).
- [16] M. Borz, M. H. Mammez, I. Blum, J. Houard, G. D. Costa, F. Delaroche, S. Idlahcen, A. Haboucha, A. Hideur, V. I. Kleshch, A. N. Obraztsov, and A. Vella, Photoassisted and multiphoton emission from single-crystal diamond needles, *Nanoscale* **11**, 6852 (2019).
- [17] B. Piglosiewicz, S. Schmidt, D. J. Park, J. Vogelsang, P. Groß, C. Manzoni, P. Farinello, G. Cerullo, and C. Lienau, Carrier-envelope phase effects on the strong-field photoemission of electrons from metallic nanostructures, *Nat. Photonics* **8**, 37 (2014).
- [18] P. Rácz, S. E. Irvine, M. Lenner, A. Mitrofanov, A. Baltuška, A. Y. Elezzabi, and P. Dombi, Strong-field plasmonic electron acceleration with few-cycle, phase-stabilized laser pulses, *Appl. Phys. Lett.* **98**, 111116 (2011).
- [19] J. Budai, Z. Pápa, P. Petrik, and P. Dombi, Ultrasensitive probing of plasmonic hot electron occupancies, *Nat. Commun.* **13**, 6695 (2022).
- [20] A. H. Zewail, 4d ultrafast electron diffraction, crystallography, and microscopy, *Annu. Rev. Phys. Chem.* **57**, 65 (2006).
- [21] C. Ropers, T. Elsaesser, G. Cerullo, M. Zavelani-Rossi, and C. Lienau, Ultrafast optical excitations of metallic nanostructures: From light confinement to a novel electron source, *New J. Phys.* **9**, 397 (2007).
- [22] R. Bormann, M. Gulde, A. Weismann, S. V. Yalunin, and C. Ropers, Tip-enhanced strong-field photoemission, *Phys. Rev. Lett.* **105**, 147601 (2010).
- [23] P. Dombi, A. Hörl, P. Rácz, I. Márton, A. Trügler, J. R. Krenn, and U. Hohenester, Ultrafast strong-field photoemission from plasmonic nanoparticles, *Nano Lett.* **13**, 674 (2013).
- [24] S. Thomas, M. Krüger, M. Förster, M. Schenk, and P. Hommelhoff, Probing of optical near-fields by electron rescattering on the 1 nm scale, *Nano Lett.* **13**, 4790 (2013).

- [25] P. Rácz, Z. Pápa, I. Márton, J. Budai, P. Wróbel, T. Stefaniuk, C. Prietl, J. R. Krenn, and P. Dombi, Measurement of nanoplasmonic field enhancement with ultrafast photoemission, *Nano Lett.* **17**, 1181 (2017).
- [26] J. Budai, Z. Pápa, I. Márton, P. Wróbel, T. Stefaniuk, Z. Márton, P. Rácz, and P. Dombi, Plasmon-plasmon coupling probed by ultrafast, strong-field photoemission with  $< 7 \text{ \AA}$  sensitivity, *Nanoscale* **10**, 16261 (2018).
- [27] B. Lovász, P. Sándor, G.-Z. Kiss, B. Bánhegyi, P. Rácz, Z. Pápa, J. Budai, C. Prietl, J. R. Krenn, and P. Dombi, Nonadiabatic nano-optical tunneling of photoelectrons in plasmonic near-fields, *Nano Lett.* **22**, 2303 (2022).
- [28] A. Grubisic, E. Ringe, C. M. Cobley, Y. Xia, L. D. Marks, R. P. Van Duyne, and D. J. Nesbitt, Plasmonic near-electric field enhancement effects in ultrafast photoelectron emission: Correlated spatial and laser polarization microscopy studies of individual Ag nanocubes, *Nano Lett.* **12**, 4823 (2012).
- [29] C. Lemke, C. Schneider, T. Leibner, D. Bayer, J. W. Radke, A. Fischer, P. Melchior, A. B. Evlyukhin, B. N. Chichkov, C. Reinhardt, M. Bauer, and M. Aeschlimann, Spatiotemporal characterization of SPP pulse propagation in two-dimensional plasmonic focusing devices, *Nano Lett.* **13**, 1053 (2013).
- [30] G. Spector, D. Kilbane, A. K. Mahro, B. Frank, S. Ristok, L. Gal, P. Kahl, D. Podbiel, S. Mathias, H. Giessen, F.-J. Meyer zu Heringdorf, M. Orenstein, and M. Aeschlimann, Revealing the subfemtosecond dynamics of orbital angular momentum in nanoplasmonic vortices, *Science* **355**, 1187 (2017).
- [31] G. G. Paulus, W. Nicklich, H. Xu, P. Lambropoulos, and H. Walther, Plateau in above threshold ionization spectra, *Phys. Rev. Lett.* **72**, 2851 (1994).
- [32] G. G. Paulus, W. Becker, and H. Walther, Classical rescattering effects in two-color above-threshold ionization, *Phys. Rev. A* **52**, 4043 (1995).
- [33] G. G. Paulus, W. Becker, W. Nicklich, and H. Walther, Rescattering effects in above-threshold ionization: A classical model, *J. Phys. B* **27**, L703 (1994).
- [34] B. Walker, B. Sheehy, K. C. Kulander, and L. F. DiMauro, Elastic rescattering in the strong field tunneling limit, *Phys. Rev. Lett.* **77**, 5031 (1996).
- [35] T. Marchenko, Y. Huismans, K. J. Schafer, and M. J. J. Vrakking, Criteria for the observation of strong-field photoelectron holography, *Phys. Rev. A* **84**, 053427 (2011).
- [36] T. Topcu and F. Robicheaux, Dichotomy between tunneling and multiphoton ionization in atomic photoionization: Keldysh parameter  $\gamma$  versus scaled frequency  $\Omega$ , *Phys. Rev. A* **86**, 053407 (2012).
- [37] S. V. Yalunin, M. Gulde, and C. Ropers, Strong-field photoemission from surfaces: Theoretical approaches, *Phys. Rev. B* **84**, 195426 (2011).
- [38] S. M. Teichmann, P. Rácz, M. F. Ciappina, J. A. Pérez-Hernández, A. Thai, J. Fekete, A. Y. Elezzabi, L. Veisz, J. Biegert, and P. Dombi, Strong-field plasmonic photoemission in the mid-IR at  $< 1 \text{ GW/cm}^2$  intensity, *Sci. Rep.* **5**, 7584 (2015).
- [39] W. P. Putnam, R. G. Hobbs, P. D. Keathley, K. K. Berggren, and F. X. Kärtner, Optical-field-controlled photoemission from plasmonic nanoparticles, *Nat. Phys.* **13**, 335 (2017).
- [40] M. Krüger, M. Schenk, P. Hommelhoff, G. Wachter, C. Lemell, and J. Burgdörfer, Interaction of ultrashort laser pulses with metal nanotips: A model system for strong-field phenomena, *New J. Phys.* **14**, 085019 (2012).
- [41] D. J. Park, B. Piglosiewicz, S. Schmidt, H. Kollmann, M. Mascheck, and C. Lienau, Strong field acceleration and steering of ultrafast electron pulses from a sharp metallic nanotip, *Phys. Rev. Lett.* **109**, 244803 (2012).
- [42] D. J. Park, B. Piglosiewicz, S. Schmidt, H. Kollmann, M. Mascheck, P. Groß, and C. Lienau, Characterizing the optical near-field in the vicinity of a sharp metallic nanoprobe by angle-resolved electron kinetic energy spectroscopy, *Ann. Phys. (Amsterdam)* **525**, 135 (2013).
- [43] P. Colosimo, G. Doumy, C. I. Blaga, J. Wheeler, C. Hauri, F. Catoire, J. Tate, R. Chirla, A. M. March, G. G. Paulus, H. G. Muller, P. Agostini, and L. F. DiMauro, Scaling strong-field interactions towards the classical limit, *Nat. Phys.* **4**, 386 (2008).
- [44] G. Z. Kiss, P. Földi, and P. Dombi, Ultrafast plasmonic photoemission in the single-cycle and few-cycle regimes, *Sci. Rep.* **12**, 3932 (2022).
- [45] See Supplemental Material at <http://link.aps.org/supplemental/10.1103/PhysRevLett.133.033801> which includes Refs. [46,47], for a detailed discussion of the numerical simulations.
- [46] B. Bánhegyi, L. Péter, P. Dombi, and Zs. Pápa, Femtosecond LIPSS on indium-tin-oxide thin films at IR wavelengths, *Appl. Opt.* **61**, 386 (2022).
- [47] C. L. Haynes, A. D. McFarland, L. Zhao, R. P. Van Duyne, G. C. Schatz, L. Gunnarsson, J. Prikulis, B. Kasemo, and M. Käll, Nanoparticle optics: The importance of radiative dipole coupling in two-dimensional nanoparticle arrays, *J. Phys. Chem. B* **107**, 7337 (2003).
- [48] J. Vogelsang, J. Robin, B. J. Nagy, P. Dombi, D. Rosenkranz, M. Schiek, P. Groß, and C. Lienau, Ultrafast electron emission from a sharp metal nanotaper driven by adiabatic nanofocusing of surface plasmons, *Nano Lett.* **15**, 4685 (2015).
- [49] R. K. Li, H. To, G. Andonian, J. Feng, A. Polyakov, C. M. Scoby, K. Thompson, W. Wan, H. A. Padmore, and P. Musumeci, Surface-plasmon resonance-enhanced multiphoton emission of high-brightness electron beams from a nanostructured copper cathode, *Phys. Rev. Lett.* **110**, 074801 (2013).